HHS Public Access

Author manuscript

Transl Stroke Res. Author manuscript; available in PMC 2020 December 01.

Published in final edited form as:

Transl Stroke Res. 2019 December ; 10(6): 705–718. doi:10.1007/s12975-019-0688-5.

Loss of endothelial laminin α5 exacerbates hemorrhagic brain injury

Jyoti Gautam, PhD[1], **Jeffrey H. Miner, PhD**[2], **Yao Yao, PhD**[1,*]

[1]Department of Pharmaceutical and Biomedical Sciences, University of Georgia, 240 W Green Street, Athens, GA, USA

[2]Division of Nephrology, Department of Medicine, Washington University School of Medicine, St. Louis, MO, USA

Abstract

Endothelial cells make laminin-411 and laminin-511. Although laminin-411 is well studied, the role of laminin-511 remains largely unknown due to the embryonic lethality of lama5$^{-/-}$ mutants. In this study, we generated endothelium-specific lama5 conditional knockout (α5-TKO) mice and investigated the biological functions of endothelial lama5 in blood brain barrier (BBB) maintenance under homeostatic conditions and the pathogenesis of intracerebral hemorrhage (ICH). First, the BBB integrity of α5-TKO mice was measured under homeostatic conditions. Next, ICH was induced in α5-TKO mice and their littermate controls using the collagenase model. Various parameters, including injury volume, neuronal death, neurological score, brain edema, BBB integrity, inflammatory cell infiltration and gliosis, were examined at various time points after injury. Under homeostatic conditions, comparable levels of IgG or exogenous tracers were detected in α5-TKO and control mice. Additionally, no differences in tight junction expression, pericyte coverage and astrocyte polarity were found in these mice. After ICH, α5-TKO mice displayed enlarged injury volume, increased neuronal death, elevated BBB permeability, exacerbated infiltration of inflammatory cells (leukocytes, neutrophils, and mononuclear cells), aggravated gliosis, unchanged brain edema, and worse neurological function, compared to the controls. These findings suggest that endothelial lama5 is dispensable for BBB maintenance under homeostatic conditions but plays a beneficial role in ICH.

Keywords

Intracerebral hemorrhage; Blood-brain barrier; Endothelial cells; Laminin

*Corresponding Author: Yao Yao, PhD, Department of Pharmaceutical and Biomedical Sciences, University of Georgia, 240 W Green Street, Athens, GA, 30602, USA. Tel: 706-542-1430; Fax: 706-542-5358; yyao@uga.edu.

Compliance with Ethical Standards

Conflict of Interest

The authors declare that they have no conflict of interest.

Ethical Approval

All applicable international. National, and/or institutional guidelines for the care and use of animals were followed. This study was approved by the Institutional Animal Care and Use Committee at the University of Georgia. This study does not contain any studies with human participants performed by any of the authors.

Introduction

The blood brain barrier (BBB) is a dynamic structure that functions to maintain brain homeostasis [1, 2]. Not only is BBB disruption a common pathophysiology of various neurological disorders, it also contributes to the pathogenesis of these diseases [3–8]. Although the BBB attracts a lot of attention due to this important function, the majority of BBB research focuses on its cellular constituents, including brain microvascular endothelial cells (BMECs), pericytes and astrocytes. Recent studies demonstrate that its non-cellular component---the basement membrane (BM) also actively participates in vascular integrity regulation [9–13].

The BM, located at the abluminal side of BMECs, is composed of highly organized extracellular matrix proteins synthesized by BMECs, pericytes and astrocytes [14–17]. Laminin, the only component required for BM formation, is a trimeric protein containing one α, one β, and one γ subunits [18, 19]. With 5 α, 4 β, and 3 γ genetic variants, many laminin isoforms exist [19, 13]. It should be noted that different cells make distinct laminin isoforms. At the BBB, astrocytes make laminin-α2β1γ1 (laminin-211) [20–22], pericytes make α4/α5-containing laminins [13, 23, 24], and BMECs synthesize laminin-411 and −511 [25, 26, 22]. Using conditional knockouts, we have reported that loss of astrocytic laminin leads to BBB disruption and spontaneous intracerebral hemorrhage (ICH) due to abnormal mural cell differentiation/maturation [27, 28]. Consistent with this finding, BBB breakdown was found in laminin-α2 null mice [21], suggesting an indispensable role of astrocytic laminin (laminin-211) in BBB maintenance. In a recent study, we also showed that loss of pericytic laminin resulted in mild BBB breakdown and hydrocephalus in a genetic background-dependent manner [24]. In addition, lama4$^{-/-}$ mice demonstrated disrupted vascular integrity at perinatal stage but not in adulthood [29], possibly due to compensatory and ubiquitous expression of lama5 in the vascular tree [30]. Although grossly normal under homeostatic conditions, these lama4$^{-/-}$ mutants had reduced T-lymphocyte extravasation and attenuated disease susceptibility & severity in multiple sclerosis [30], suggesting a critical role of lama4/lama5 in vascular integrity and disease progression in pathological conditions. Unlike lama4, lama5 global knockout results in embryonic lethality [31], preventing investigation of lama5's function at postnatal stage.

To overcome this limitation, we generated an endothelium-specific lama5 knockout line. Using these mutants, we first investigated whether endothelial lama5 is required for BBB maintenance under homeostatic conditions. Next, the role of endothelial lama5 in pathological conditions was also examined using ICH as a disease model. ICH was chosen for the following reasons: (1) it is a cerebrovascular disease that causes degradation of laminin-containing BM [32], (2) BBB integrity is tightly associated with secondary brain injury [33], and (3) it has the highest rates of mortality and disability but without effective treatments so far. We report that endothelial lama5 is dispensable for BBB maintenance under homeostatic conditions, and that loss of endothelial lama5 results in exacerbated injury at structural, biochemical, and functional levels after ICH, suggesting a beneficial role laminin-511 in ICH.

Material and Methods

Animals

The experimental protocols were approved by the Institutional Animal Care and Use Committee at the University of Georgia and were in accordance with the NIH guidelines for the care and use of animals. Laminin-α5$^{flox/flox}$ mice [34] were crossed with the Tie2-Cre^{+} transgenic line (Jackson Lab: 008863) to generate laminin α5$^{flox/flox}$:Tie2-Cre^{+} (α5-TKO) mice. Littermate laminin α5$^{flox/flox}$ and laminin α5$^{flox/+}$:Tie2-Cre^{+} mice were used as controls. Mice of both genders at the age of 6–8 weeks were used in this study. All mice were housed in the animal facility at the University of Georgia with free access to water and food.

ICH Model

Mice were anesthetized by intraperitoneal injection of avertin (500 mg/kg of body weight). ICH was induced by intracerebral injection of collagenase as described previously [35–39]. Briefly, mice were placed in a stereotaxic frame (Stoelting Co, IL, USA). A 24-gauge needle was inserted through a burr hole into the striatum at the following coordinates: 0.2 mm anterior to the bregma, 2.2 mm lateral to the midline, 3.7 mm in depth below the skull. ICH was induced by administration of collagenase (type VII-S; Sigma, St. Louis, USA; 0.225U in 0.5 μl saline) over 5 minutes. After injection, the needle was kept in place for 10 minutes to prevent reflux. On 2, 5, and 10 days post injury (dpi), mice were transcardially perfused with phosphate-buffered saline (PBS) and/or 4% paraformaldehyde (PFA), and the brains were sectioned using a cryostat (Microm HM 550, Thermoscientific, USA).

Histology

Hematoxylin staining and Fluoro-Jade C (FJC) staining were performed to visualize brain injury and degenerating neurons, respectively, as described previously [40, 35, 41]. Brain injury volume was quantified using NIS-Elements D3.0 software as follow: injury volume (mm^3) = sum of injury area × section thickness. FJC^{+} cells were counted in six-eight sections/mouse, using three fields immediately adjacent to the hematoma. The numbers of degenerating cells were expressed as cells/field.

RT-PCR

Total RNA was extracted from bone marrow cells and peripheral blood leukocytes freshly isolated from control and α5-TKO mice using Trizol (Invitrogen, USA), according to the manufacturer's instructions. Equal amount of total RNA was subjected to reverse transcription using the SuperScript III First-Strand Synthesis System (Invitrogen, USA). The expression of lama5 and β-Actin were determined following standard PCR procedure. The following primers were used in this study. Lama5: 5'-AGCCTCTCGACTCACCTCAT-3', 5'-GCACCTGTTCTCTCGTGTCA-3'; β-Actin: 5'-ACAGCTGAGAGGGAAATCGT-3', 5'-TGCTAGGAGCCAGAGCAGTA-3'.

Immunohistochemistry/Immunofluorescence

Standard immunohistochemistry and immunofluorescence protocols were used to examine protein expression. Primary antibodies used in this study included: Rabbit anti-Laminin α5 (1:800, generated as described previously [42]), Rat anti-Laminin α2 (1:400, Sigma, USA), Goat anti-Laminin α4 (1:400, R&D, USA), Rat anti-CD31 (1:100, BD Biosciences, USA), Mouse anti-Claudin-5 (1:200, Invitrogen, USA), Rabbit anti-ZO-1 (1:400, Thermofisher, USA), Rat anti-PDGFRβ (1:200, eBioscience, USA), Rabbit anti-AQP4 (1:500, Millipore, USA), IB4–488 (1:200, Thermofischer, USA), Rat anti-Ly6G (1:200; Biolegend, USA), Rat anti-CD68 (1:200, Biolegend, USA), Rabbit anti-glial fibrillary acidic protein (GFAP, 1:400, Stem cell, USA), and Rabbit anti-Iba1 (1:500; Wako Inc, USA). The fluorescence intensity of immunoreactivity and the number of immune-positive cells were calculated using the ImageJ software (NIH, USA). For quantifications, 3–5 random fields around the hematoma per section, 5 non-consecutive sections per animal, and at least 3 animals were used.

Angioarchitecture analysis

Vessel density, vessel length, and branching index were analyzed using IB4 staining and the AngioTool software as described previously [43–45]. Vessel density was defined as the percentage of IB4-positive area over total area. Vessel length is defined as the mean length of all vessels in the image. Branching Index is defined as the number of vessel junctions normalized per unit area. Changes in α5-TKO mice were normalized to that in controls. In these analyses, 3 random images from each section, 8 sections from each mouse, and 3 mice (n=3) were used for quantifications.

In vivo permeability assay

BBB permeability was examined using *in vivo* permeability assay as described previously [46–48, 39]. Briefly, sterile Evans blue solution (2% in saline, 80μl) and 4 kD-FITC-Dextran (25 mg/ml, 50μl) were injected intravenously into control and mutant mice. After 6 hours, these mice were transcardially perfused with 50 ml saline. The brains were then collected and cut into left and right hemispheres. Each hemisphere was carefully weighed and homogenized in 800μl of PBS and centrifuged at 13,200 rpm for 20 minutes at 4 °C. For FITC-Dextran, the supernatant was collected and read in a fluorescent plate reader (Molecular devices-SpectraMax, California, USA) at 485/528nm. For Evans blue, the supernatant was collected and read in a spectrophotometer (Molecular devices-SpectraMax, California, USA) at 620nm. Each sample was measured in triplicates and the average of these technical replicates was used as one biological replicate. Six animals per group were used for quantification. The results were normalized to the controls.

Brain Edema Measurement

Brain edema was measured using the wet weight and dry weight method as described previously [35, 41, 49, 39]. Briefly, brains were collected at 2, 5 and 10 dpi and divided into left and right hemispheres. These hemispheres and cerebellum (internal control) were weighed immediately (wet weight) using an analytical balance. The samples were then dried at 95°C for 24 h and reweighted (dry weight). Brain edema was calculated as follow: Brain edema = (wet weight − dry weight)/wet weight × 100.

Neurological Deficit

Neurological deficit was examined using a modified 28-point scoring system, which assesses body symmetry, gait, climbing, circling behavior, front limb symmetry, and compulsory circling, as described previously [50, 51, 35]. A higher score indicates more severe neurological deficit. The person scoring these mice was blinded to the genotypes.

Statistics

All data were presented as mean ± SD. Student's t-test was used to analyze differences between two groups. One-Way ANOVA followed by Newman-Keuls test was used for data analyses of more than two groups using GraphPad Prism (GraphPad Software, San Diego, CA, USA). $p<0.05$ was considered to be significant.

Results

Lama5 is selectively ablated in endothelial cells in α5-TKO mice

By crossing lama5 floxed mice with Tie2-Cre transgenic line, we generated endothelium-specific lama5 knockout (α5-TKO) mice. The α5-TKO were born at expected Mendelian ratio without gross abnormalities (not shown). To validate the specificity and efficiency of endothelial lama5 abrogation, we performed immunochemical analyses against lama2, lama4 and lama5. These laminin α subunits were chosen because astrocytes predominantly make laminin-211 [20–22], whereas endothelial cells synthesize laminin-411 and −511 [25, 26, 22]. Immunohistochemistry revealed strong lama2, lama4 and lama5 signals in control brains (Fig. 1a). Although lama2 and lama4 were found in α5-TKO brains, lama5 was barely detected in these mutants (Fig. 1a). The residual level of lama5 in α5-TKO brains is probably from mural cells, which have been shown to also synthesize lama5 [13, 23, 24]. Quantifications showed that lama5 (fold change: 1.00±0.11 in controls versus 0.08±0.03 in α5-TKO mice), but not lama2 (fold change: 1.00±0.08 in controls versus 0.98±0.06 in α5-TKO mice) or lama4 (fold change: 1.00±0.07 in controls versus 0.99±0.06 in α5-TKO mice), intensity was significantly reduced in α5-TKO mice compared to the controls (Fig. 1b). These results suggest that endothelial lama5 is indeed abrogated in α5-TKO mutants, and that loss of endothelial lama5 does not affect the expression of lama2 or lama4. In addition to endothelial cells, the Tie2-Cre transgenic line has been reported to induce recombination in hematopoietic cells [52–54]. To investigate if lama5 is ablated in hematopoietic cells, we examined lama5 expression in bone marrow cells and peripheral blood leukocytes isolated from control and α5-TKO mice. We failed to detect lama5 in either bone marrow cells or peripheral blood leukocytes independent of the genotype (Fig. 1c), indicating that these cells do not express lama5. Together, these findings suggest that lama5 is abrogated in endothelial cells specifically in α5-TKO mice, and that any phenotypes observed in these mutants are due to loss of lama5 in endothelial cells.

Brain angioarchitecture and BBB integrity are unaffected in α5-TKO mice under homeostatic conditions

To determine if loss of endothelial lama5 affects brain angioarchitecture, we performed immunostaining against IB4 (endothelial marker, Fig. 2a) and analyzed vessel density, vessel

length, and branching index in control and α5-TKO brains. Compared to the controls, no significant differences in vessel density (fold change: 1.00±0.12 in controls versus 0.82±0.17 in α5-TKO mice), vessel length (fold change: 1.00±0.18 in controls versus 0.94±0.23 in α5-TKO mice), and branching index (fold change: 1.00±0.34 in controls versus 0.85±0.49 in α5-TKO mice) were detected in α5-TKO mice (Fig. 2b-d), strongly suggesting that loss of endothelial lama5 does not affect brain angioarchitecture. To investigate if loss of endothelial lama5 affects BBB permeability under homeostatic conditions, we first examined the leakage of IgG (~150kDa) into brain parenchyma. Immunohistochemistry showed absence of IgG in both control and α5-TKO brains (Fig. 2e). Quantification revealed similar levels of IgG in control and α5-TKO brains (fold change: 1.00±0.22 in controls versus 1.12±0.25 in α5-TKO mice) (Fig. 2f), suggesting that the BBB is impermeable to molecules of 150kDa or larger in α5-TKO mice. To determine if the BBB is leaky to smaller molecules, we also performed BBB permeability assay using Evans blue (~66kDa due to albumin binding) and FITC-Dextran (4kDa). Comparable levels of Evans blue (fold change: 1.00±0.13 in controls versus 1.07±0.16 in α5-TKO mice) and FITC-Dextran (fold change: 1.00±0.07 in controls versus 1.04±0.07 in α5-TKO mice) were found in control and α5-TKO brains (Fig. 2g, h), strongly suggesting that endothelial lama5 is dispensable for BBB maintenance under homeostatic conditions.

TJP expression, pericyte coverage, and astrocyte polarity are unaffected in α5-TKO mice

TJPs seal gaps between endothelial cells, limiting paracellular transport [55, 56]. Immunohistochemistry showed that Claudin-5 and ZO-1 co-localized with each other in both control and α5-TKO brains (Fig. 3a). Quantifications revealed comparable levels of Claudin-5 (fold change: 1.00±0.13 in controls versus 1.03±0.11 in α5-TKO mice) and ZO-1 (fold change: 1.00±0.12 in controls versus 0.93±0.08 in α5-TKO mice) in control and α5-TKO mice (Fig. 3b), suggesting that TJP expression is not affected in these mutants. Accumulating evidence shows that pericyte coverage on capillaries positively correlates with BBB integrity [57–60]. In both control and α5-TKO brains, PDGFRβ (pericyte marker) co-localized with IB4 (blood vessel marker) (Fig. 3c). Quantifications demonstrated that pericyte coverage, defined as the percentage of $IB4^+$ capillary area covered by $PDGFR\beta^+$ pericyte area, was unaltered in α5-TKO brains compared to the controls (76.0±4.2% in controls versus 74.6±4.0% in α5-TKO mice) (Fig. 3d). Astrocytes cover CNS microvessels using their endfeet, where AQP4 is exclusively expressed [61, 58, 27, 24]. To determine if AQP4 distribution/expression is affected, we performed immunohistochemical analysis against AQP4 and CD31. In both control and α5-TKO mice, AQP4 is located at the abluminal side of CD31 (Fig. 3e), indicating that the polarized distribution of AQP4 is not disrupted in α5-TKO mice. Quantification revealed no significant difference in AQP4 fluorescence intensity between control and α5-TKO mice (fold change: 1.00±0.10 in controls versus 0.99±0.09 in α5-TKO mice) (Fig. 3f), suggesting that AQP4 expression is unaltered in the mutants. Together, these results suggest that loss of lama5 in endothelial cells does not affect TJP expression, pericyte coverage, and astrocyte polarity.

α5-TKO mice have increased injury volume after ICH

To investigate the role of endothelial lama5 in the pathogenesis of hemorrhagic stroke, we induced intracerebral hemorrhage (ICH) in α5-TKO mice and their littermate controls, and

assessed various parameters at 2, 5 and 10 days post injury (dpi). Injury volume peaked at 2 dpi and gradually decreased at 5 and 10 dpi in control mice (Fig. 4a, b). Similar trend was observed in α5-TKO mice (Fig. 4a, b). Compared to the controls, α5-TKO mice showed significantly enlarged injury volume at 2 (15.63±2.10mm^3 in controls versus 25.47±3.46mm^3 in α5-TKO mice) and 5 dpi (10.75±1.72mm^3 in controls versus 16.74±3.43mm^3 in α5-TKO mice) (Fig. 4b). Although not statistically significant, increased injury volume was also observed in α5-TKO mice at 10 dpi (4.60±1.88mm^3 in controls versus 7.06±3.64mm^3 in α5-TKO mice) (Fig. 4b). High-magnification images of hematoxylin staining at the injury sites were shown in Supplementary Fig. 1 (Online Resource 1). These data suggest that endothelial lama5 negatively regulates injury volume after ICH.

α5-TKO mice show enhanced neuronal death after ICH

To examine neuronal death after ICH, we performed FJC staining, which labels degenerating neurons specifically [62]. In control mice, the number of FJC^+ cells peaked at 2 dpi and gradually decreased over time (Fig. 4c, d). In α5-TKO mice, however, the number of FJC^+ cells remained high at 5 dpi (Fig. 4c, d). Compared to the controls, α5-TKO mice showed higher number of FJC^+ cells at all time points examined, but statistical significance was only reached at 5 dpi (63.15±9.79, 52.10±12.45, and 35.93±11.99 in controls versus 81.31±11.52, 82.26±16.03, and 50.54±10.21 in α5-TKO mice at 2, 5, and 10 dpi) (Fig. 4d). These results suggest an important role of endothelial lama5 in neuronal death after ICH.

α5-TKO mice have exacerbated BBB disruption after ICH

Since BBB disruption actively contributes to secondary brain injury after ICH [33], we also examined BBB integrity in α5-TKO and control mice at various time points after ICH. First, we analyzed the leakage of IgG into brain parenchyma by immunohistochemistry. Due to the rupture of blood vessels caused by collagenase, we do not expect different IgG levels in the brain at early time points after ICH. Consistent with this speculation, similar levels of IgG were detected in control and α5-TKO brains at 2 dpi (mean intensity: 12.94±1.71 in controls versus 9.98±3.23 in α5-TKO mice) (Fig. 5a, b). At 5 dpi, however, significantly higher levels of IgG were found in α5-TKO brains (mean intensity: 8.04±6.35 in controls versus 21.20±3.16 in α5-TKO mice) (Fig. 5a, b). Similarly, increased IgG leakage was found in α5-TKO mice at 10 dpi, although it did not reach statistical significance (mean intensity: 4.03±3.70 in controls versus 6.65±1.61 in α5-TKO mice) (Fig. 5a, b). Next, we further validated this result by examining the leakage of intravenously injected tracers (Evans blue and FITC-Dextran) in α5-TKO and control mice at 5 dpi. Consistent with IgG data, substantially higher levels of Evans blue (fold change: 1.00±0.81 in controls versus 2.67±1.62 in α5-TKO mice) and FITC-Dextran (fold change: 1.00±0.47 in controls versus 1.80±0.53 in α5-TKO mice) were detected in α5-TKO brains at 5 dpi (Fig. 5c, d). Together, these findings suggest a critical role of endothelial lama5 in BBB maintenance after ICH.

α5-TKO mice demonstrate increased inflammatory cell infiltration after ICH

With exacerbated BBB disruption, we expect enhanced inflammatory cell infiltration. To assess inflammatory cell infiltration, we examined the extravasation of neutrophils and monocytes/macrophages in brain parenchyma after ICH by immunohistochemistry. In

control mice, $Ly6G^+$ neutrophil counts peaked at 2 and 5 dpi and substantially diminished by 10 dpi (Fig. 6a). In α5-TKO mice, however, the number of $Ly6G^+$ neutrophils remained high at 10 dpi (Fig. 6a). Quantification revealed significantly more $Ly6G^+$ neutrophils at 10 dpi in α5-TKO mice (41.98±9.91 in controls versus 77.68±10.82 in α5-TKO mice), although no difference was found at 2 (74.21±16.97 in controls versus 72.22±47.71 in α5-TKO mice) and 5 dpi (70.01±11.73 in controls versus 55.51±12.63 in α5-TKO mice) (Fig. 6b). Unlike neutrophils, monocyte/macrophage numbers gradually increased after ICH, peaked at 5 dpi, and remained high at 10 dpi in both control and α5-TKO mice (Fig. 6c). Compared to the controls, however, α5-TKO mice demonstrated significantly higher number of $CD68^+$ monocytes/macrophages at all three time points after ICH (48.48±13.00, 100.24±2.42, and 85.12±7.89 in controls versus 71.44±10.05, 128.74±9.13, and 120.49±8.71 in α5-TKO mice at 2, 5, and 10 dpi) (Fig. 6d). It should be noted that CD68 does not distinguish monocytes/macrophages or brain-resident microglia. These results strongly suggest that endothelial lama5 negatively regulates inflammatory cell extravasation after ICH.

α5-TKO mice have enhanced reactive astrogliosis and microglial activation after ICH

Reactive astrogliosis and microglial activation play important roles in brain injury after ICH [63, 64, 35]. To access the role of lama5 in this process, we performed immunohistochemistry against GFAP in control and α5-TKO mice at various time points after ICH. Typical morphology of activated astrocytes was observed in both control and α5-TKO brains (Fig. 7a). Quantification revealed significantly elevated GFAP fluorescence intensity in α5-TKO mice at 2 and 5 but not 10 dpi (mean intensity: 10.53±0.78, 10.02±0.24, and 13.65±0.51 in controls versus 13.15±1.31, 13.63±1.30, and 14.58±1.38 in α5-TKO mice at 2, 5, and 10 dpi) (Fig. 7b), suggesting enhanced reactive astrogliosis in these mutants. In addition to astrocytes, microglia also play an important role in brain injury after ICH [63, 64, 35]. Iba-1 immunostaining demonstrated typical ameboid morphology at 2 and 5 dpi in both control and α5-TKO mice (Fig. 7c), indicating activated microglia at early time points after ICH. Although Iba-1^+ microglia returned to ramified morphology (resting/semi-activated) by 10 dpi in the controls, they remained the ameboid morphology at this time point in α5-TKO brains (Fig. 7c), suggesting abnormal microglial activation in α5-TKO mice. Quantification displayed significantly higher number of Iba-1^+ microglia at 2 and 10 dpi in α5-TKO mice compared to the controls (25.51±2.76, 63.78±8.52, and 44.44±9.01 in controls versus 43.29±7.98, 62.59±13.62, and 77.39±18.06 in α5-TKO mice at 2, 5, and 10 dpi) (Fig. 7d), suggesting exacerbated microglial activation in α5-TKO mice. It should be noted that Iba-1 is not a microglia-specific marker. It also labels brain resident macrophages and infiltrating monocytes, in addition to microglia [65, 66].

α5-TKO mice show exacerbated brain edema after ICH

To determine if endothelial lama5 affects brain edema after ICH, we examined brain water contents in control and α5-TKO mice. Compared to the contralateral hemisphere, the ipsilateral hemisphere showed significantly higher water contents in both control and α5-TKO mice at 2 dpi (Fig. 7e), indicating successful induction of ICH. However, no significant difference in brain water content was observed in the ipsilateral hemisphere between

genotypes (Fig. 7e), suggesting that endothelial lama5 plays a minimal role in brain edema after ICH.

α5-TKO mice demonstrate worse neurological function after ICH

To assess the role of endothelial lama5 in neurological function after ICH, neurological deficit score was measured in control and α5-TKO mice at 2, 5, and 10 dpi. In control mice, neurological deficit score gradually decreased over time (Fig. 7f), indicating recovery. In α5-TKO mice, however, this score remained high at later time points (Fig. 7f). Higher neurological deficit score was found in α5-TKO mice at all time points examined, although significance was only reached at 10 dpi (9.24±2.11, 8.80±1.87, and 6.14±1.57 in controls versus 11.09±1.81, 9.11±2.62, and 11.00±3.54 in α5-TKO mice at 2, 5, and10 dpi) (Fig. 7f). These findings suggest that loss of endothelial lama5 compromises neurological function recovery after ICH.

Discussion

Unlike astrocytic laminin conditional knockout mice [27, 28], α5-TKO mice failed to show BBB disruption under homeostatic conditions. This result is consistent with previous reports using a different lama5 floxed line [67, 68], highlighting a dispensable role of endothelial lama5 (laminin-511) in BBB maintenance under homeostatic conditions. The absence of BBB leakage in α5-TKO mice suggests the existence of potential compensation. One possibility is that the loss of endothelial lama5 (laminin-511) is functionally compensated by laminin-411, the other laminin isoform synthesized by endothelial cells, although laminin-411 expression is not up-regulated in α5-TKO mutants. The spatial and temporal distribution of lama4 and lama5 in the vasculature supports this possibility. Specifically, lama4 is ubiquitously expressed in all types of vessels starting in embryonic stage, while lama5 has a patchy distribution pattern in post-capillary venules starting in postnatal stage [30]. It should be noted that, however, distinct functions of laminin-511 and laminin-411 in immune cell extravasation have also been proposed [30, 67, 69–71]. Another possibility is that the loss of endothelial lama5 (laminin-511) is compensated by laminin isoforms from other cells (e.g. pericytes). Although loss of pericytic laminin leads to mild BBB compromise and hydrocephalus in a mixed genetic background [24], our unpublished data show that pericytic laminin-deficient mice are grossly normal at young age in C57/Bl6 background. Like endothelial cells, pericytes predominantly synthesize α4/α5-containing laminins [13, 23, 24]. Given the close proximity of endothelium- and pericyte-derived laminins in the BM [13, 32] and the same laminin α subunits, it is logical to hypothesize that pericyte-derived α5-containing laminins are able to compensate for the loss of endothelial lama5 (laminin-511). Transgenic mice with simultaneous loss of laminin-511/411 in endothelium and those with laminin deficiency in multiple cell types will help determine which laminin isoform(s) is involved in the compensation.

Although α5-TKO mice have intact BBB integrity under homeostatic conditions, they show increased IgG leakage and enhanced accumulation of intravenously injected tracers in brain parenchyma after ICH, suggesting exacerbated BBB disruption. Consistent with this finding, significantly more $Ly6G^+$ neutrophils and $CD68^+$ mononuclear cells were observed in α5-

TKO mice, indicating an inhibitory role of endothelial lama5 (laminin-511) in inflammatory cell extravasation. This conclusion is supported by various previous reports. For example, increased neutrophil extravasation and compromised endothelial junction/barrier function were observed in the cremaster muscle of α5-TKO mice after intrascrotal injection of TNF-α [67]. Similarly, reduced T lymphocyte infiltration was found in lama4 null mice, which showed elevated and ubiquitous expression of lama5 in the vasculature, in multiple sclerosis [30]. In addition, transmigration of inflammatory cells primarily occurs in lama5^{low} regions [71, 70, 69], and administration of murine laminin alpha chain peptides inhibits leukocyte accumulation in rats after ischemic stroke [72]. Together, these findings suggest that laminin-511 negatively regulates inflammatory cell infiltration under pathological conditions. The molecular mechanism, however, remains largely unknown.

In addition to exacerbated BBB disruption, we also found enlarged injury volume, increased neuronal death, and more severe neurological dysfunction in the α5-TKO mice after ICH. These findings are in accordance with previous studies showing that: (1) laminin is required for the survival of hippocampal neurons and laminin degradation results in neuronal death in the hippocampus [73, 74], and (2) lama5 stabilizes synapses during development and deletion of lama5 in neurons leads to age-dependent synapse loss and behavioral defects [75]. These results suggest that laminin-511 plays an indispensable role in neuronal survival and function.

Furthermore, we observed increased GFAP intensity and elevated Iba-1^{+} cells in α5-TKO mice after ICH, indicating aggravated astrocyte/microglial activation. Consistent with this observation, it has been shown that laminin inhibits astrocyte growth induced by IL-1β [76] and that retinal microglia become hyperactivated upon loss of laminin γ3 [77]. In addition, laminin-111 has also been found to sustain the bipolar/rod morphology of microglia, which is involved in CNS repair [78]. These results suggest that laminins negatively regulate gliosis either directly or indirectly. It should be noted, however, that Iba-1 also marks brain resident macrophages and infiltrating monocytes, in addition to microglia [65, 66]. Thus, we were unable to distinguish these cells in this study.

In this study, collagenase VII was used to induce ICH. This model has many advantages compared to the autologous blood model [79], an alternative ICH model [80, 81]. For example, it induces small vessel rupture and mimics ICH pathology that occurs naturally in humans, such as intraparenchymal bleeding and subsequent hematoma expansion from continuous bleeding [82–84, 51]. This is consistent with the observations that: (1) hematoma size remains stable in the autologous blood model but increases overtime in the collagenase model [85–87], and (2) hematoma resolution is faster in the autologous blood model than the collagenase model [85, 87]. In addition, the collagenase model can also provide information on the response of brain tissue to bleeding and the role of basal lamina in BBB integrity. Accumulating evidence shows that intracerebral injection of collagenase damages the basal lamina (ECM destruction and thickening/widening of the basal lamina), leading to enhanced BBB permeability [82, 88, 89, 51, 40, 35]. The collagenase model, on the other hand, also has some disadvantages [79]. Unlike the autologous blood model, the collagenase model adds a confounding factor (exogenous collagenase) to the system [83, 90, 80]. It has been shown that collagenase amplifies inflammatory response and has neurotoxic effects at high

doses [91]. For instance, neutrophil infiltration and neuronal death are observed in the collagenase model but not in the autologous blood model at late time points (e.g. 7–21 days after injury) [85, 92–94]. Since collagenase affects multiple targets in the brain (ECM, blood vessels, inflammatory response), it is difficult to dissect its effects on the ECM and subsequent pathological processes triggered by blood inflow into the brain.

Together, our results show that endothelial lama5 is dispensable for BBB maintenance under homeostatic conditions but plays a beneficial role in ICH. The protective role of endothelial lama5 is possibly due to its effects in BBB integrity, neuronal survival/function, and astrocyte/microglial activation.

Supplementary Material

Refer to Web version on PubMed Central for supplementary material.

Acknowledgments

We thank the Yao Lab members for discussions and suggestions.

Funding

This study was supported, in part, by the American Heart Association grant 16SDG29320001 (to YY) and NIH R01DK078314 (to JHM).

References

1. Persidsky Y, Ramirez SH, Haorah J, Kanmogne GD. Blood-brain barrier: structural components and function under physiologic and pathologic conditions. J Neuroimmune Pharmacol. 2006;1(3):223–36. doi:10.1007/s11481-006-9025-3. [PubMed: 18040800]
2. Liebner S, Dijkhuizen RM, Reiss Y, Plate KH, Agalliu D, Constantin G. Functional morphology of the blood-brain barrier in health and disease. Acta neuropathologica. 2018;135(3):311–36. doi: 10.1007/s00401-018-1815-1. [PubMed: 29411111]
3. Zhao Z, Nelson AR, Betsholtz C, Zlokovic BV. Establishment and Dysfunction of the Blood-Brain Barrier. Cell. 2015;163(5):1064–78. doi:10.1016/j.cell.2015.10.067. [PubMed: 26590417]
4. Zlokovic BV. The blood-brain barrier in health and chronic neurodegenerative disorders. Neuron. 2008;57(2):178–201. doi:10.1016/j.neuron.2008.01.003. [PubMed: 18215617]
5. Zipser BD, Johanson CE, Gonzalez L, Berzin TM, Tavares R, Hulette CM et al. Microvascular injury and blood-brain barrier leakage in Alzheimer's disease. Neurobiology of aging. 2007;28(7): 977–86. doi:S0197-4580(06)00175-8 [pii] 10.1016/j.neurobiolaging.2006.05.016. [PubMed: 16782234]
6. van Vliet EA, da Costa Araujo S, Redeker S, van Schaik R, Aronica E, Gorter JA. Blood-brain barrier leakage may lead to progression of temporal lobe epilepsy. Brain : a journal of neurology. 2007;130(Pt 2):521–34. doi:awl318 [pii] 10.1093/brain/awl318. [PubMed: 17124188]
7. Marchi N, Angelov L, Masaryk T, Fazio V, Granata T, Hernandez N et al. Seizure-promoting effect of blood-brain barrier disruption. Epilepsia. 2007;48(4):732–42. doi:EPI988 [pii] 10.1111/j. 1528-1167.2007.00988.x. [PubMed: 17319915]
8. Wardlaw JM, Doubal F, Armitage P, Chappell F, Carpenter T, Munoz Maniega S et al. Lacunar stroke is associated with diffuse blood-brain barrier dysfunction. Annals of neurology. 2009;65(2): 194–202. doi:10.1002/ana.21549. [PubMed: 19260033]
9. Ohashi KL, Tung DK, Wilson J, Zweifach BW, Schmid-Schonbein GW. Transvascular and interstitial migration of neutrophils in rat mesentery. Microcirculation. 1996;3(2):199–210. [PubMed: 8839442]

10. Yadav R, Larbi KY, Young RE, Nourshargh S. Migration of leukocytes through the vessel wall and beyond. Thrombosis and haemostasis. 2003;90(4):598–606. doi:10.1160/TH03-04-0220. [PubMed: 14515179]
11. Hoshi O, Ushiki T. Neutrophil extravasation in rat mesenteric venules induced by the chemotactic peptide N-formyl-methionyl-luecylphenylalanine (fMLP), with special attention to a barrier function of the vascular basal lamina for neutrophil migration. Arch Histol Cytol. 2004;67(1):107–14. [PubMed: 15125027]
12. Bixel MG, Petri B, Khandoga AG, Khandoga A, Wolburg-Buchholz K, Wolburg H et al. A CD99-related antigen on endothelial cells mediates neutrophil but not lymphocyte extravasation in vivo. Blood. 2007;109(12):5327–36. doi:10.1182/blood-2006-08-043109. [PubMed: 17344467]
13. Nirwane A, Yao Y. Laminins and their receptors in the CNS. Biological reviews of the Cambridge Philosophical Society. 2018. doi:10.1111/brv.12454.
14. Vracko R, Benditt EP. Capillary basal lamina thickening. Its relationship to endothelial cell death and replacement. The Journal of cell biology. 1970;47(1):281–5. [PubMed: 5513555]
15. Kalluri R Basement membranes: structure, assembly and role in tumour angiogenesis. Nature reviews Cancer. 2003;3(6):422–33. doi:10.1038/nrc1094. [PubMed: 12778132]
16. LeBleu VS, Macdonald B, Kalluri R. Structure and function of basement membranes. Exp Biol Med (Maywood). 2007;232(9):1121–9. doi:10.3181/0703-MR-72. [PubMed: 17895520]
17. Yao Y Extracellular Matrix in Stroke In: Jiang W, Yu W, Qu Y, Shi Z, Luo B, Zhang JH, editors. Cerebral Ischemic Reperfusion Injuries (CIRI): Bench Research and Clinical Implications. Cham: Springer International Publishing; 2018 p. 121–44.
18. Colognato H, Yurchenco PD. Form and function: the laminin family of heterotrimers. Developmental dynamics : an official publication of the American Association of Anatomists. 2000;218(2):213–34. doi:10.1002/(SICI)1097-0177(200006)218:2<213::AID-DVDY1>3.0.CO;2-R [pii] 10.1002/(SICI)1097–0177(200006)218:2<213::AID-DVDY1>3.0.CO;2-R. [PubMed: 10842354]
19. Yao Y Laminin: loss-of-function studies. Cell Mol Life Sci. 2017;74(6):1095–115. doi:10.1007/s00018-016-2381-0. [PubMed: 27696112]
20. Jucker M, Tian M, Norton DD, Sherman C, Kusiak JW. Laminin alpha 2 is a component of brain capillary basement membrane: reduced expression in dystrophic dy mice. Neuroscience. 1996;71(4):1153–61. doi:0306-4522(95)00496-3 [pii]. [PubMed: 8684619]
21. Menezes MJ, McClenahan FK, Leiton CV, Aranmolate A, Shan X, Colognato H. The Extracellular Matrix Protein Laminin alpha2 Regulates the Maturation and Function of the Blood-Brain Barrier. The Journal of neuroscience : the official journal of the Society for Neuroscience. 2014;34(46):15260–80. doi:10.1523/JNEUROSCI.3678-13.2014.
22. Hannocks MJ, Pizzo ME, Huppert J, Deshpande T, Abbott NJ, Thorne RG et al. Molecular characterization of perivascular drainage pathways in the murine brain. Journal of cerebral blood flow and metabolism : official journal of the International Society of Cerebral Blood Flow and Metabolism. 2018;38(4):669–86. doi:10.1177/0271678X17749689.
23. Stratman AN, Malotte KM, Mahan RD, Davis MJ, Davis GE. Pericyte recruitment during vasculogenic tube assembly stimulates endothelial basement membrane matrix formation. Blood. 2009;114(24):5091–101. doi:10.1182/blood-2009-05-222364 blood-2009–05-222364 [pii]. [PubMed: 19822899]
24. Gautam J, Zhang X, Yao Y. The role of pericytic laminin in blood brain barrier integrity maintenance. Sci Rep. 2016;6:36450. doi:10.1038/srep36450. [PubMed: 27808256]
25. Sixt M, Engelhardt B, Pausch F, Hallmann R, Wendler O, Sorokin LM. Endothelial cell laminin isoforms, laminins 8 and 10, play decisive roles in T cell recruitment across the blood-brain barrier in experimental autoimmune encephalomyelitis. The Journal of cell biology. 2001;153(5):933–46. [PubMed: 11381080]
26. Sorokin LM, Pausch F, Frieser M, Kroger S, Ohage E, Deutzmann R. Developmental regulation of the laminin alpha5 chain suggests a role in epithelial and endothelial cell maturation. Developmental biology. 1997;189(2):285–300. doi:S0012-1606(97)98668-1 [pii] 10.1006/dbio.1997.8668. [PubMed: 9299121]

27. Yao Y, Chen ZL, Norris EH, Strickland S. Astrocytic laminin regulates pericyte differentiation and maintains blood brain barrier integrity. Nature communications. 2014;5:3413. doi:10.1038/ncomms4413 ncomms4413 [pii].
28. Chen ZL, Yao Y, Norris EH, Kruyer A, Jno-Charles O, Akhmerov A et al. Ablation of astrocytic laminin impairs vascular smooth muscle cell function and leads to hemorrhagic stroke. J Cell Biol. 2013;202(2):381–95. doi:10.1083/jcb.201212032. [PubMed: 23857767]
29. Thyboll J, Kortesmaa J, Cao R, Soininen R, Wang L, Iivanainen A et al. Deletion of the laminin alpha4 chain leads to impaired microvessel maturation. Mol Cell Biol. 2002;22(4):1194–202. [PubMed: 11809810]
30. Wu C, Ivars F, Anderson P, Hallmann R, Vestweber D, Nilsson P et al. Endothelial basement membrane laminin α5 selectively inhibits T lymphocyte extravasation into the brain. Nature medicine. 2009;15(5):519–27.
31. Miner JH, Cunningham J, Sanes JR. Roles for laminin in embryogenesis: exencephaly, syndactyly, and placentopathy in mice lacking the laminin alpha5 chain. The Journal of cell biology. 1998;143(6):1713–23. [PubMed: 9852162]
32. Yao Y Basement membrane and stroke. Journal of Cerebral Blood Flow & Metabolism. 2018:In press.
33. Keep RF, Hua Y, Xi G. Intracerebral haemorrhage: mechanisms of injury and therapeutic targets. The Lancet Neurology. 2012;11(8):720–31. doi:10.1016/S1474-4422(12)70104-7. [PubMed: 22698888]
34. Nguyen NM, Kelley DG, Schlueter JA, Meyer MJ, Senior RM, Miner JH. Epithelial laminin alpha5 is necessary for distal epithelial cell maturation, VEGF production, and alveolization in the developing murine lung. Developmental biology. 2005;282(1):111–25. doi:10.1016/j.ydbio.2005.02.031. [PubMed: 15936333]
35. Yao Y, Tsirka SE. The CCL2-CCR2 system affects the progression and clearance of intracerebral hemorrhage. Glia. 2012;60(6):908–18. doi:10.1002/glia.22323. [PubMed: 22419223]
36. Klahr AC, Dickson CT, Colbourne F. Seizure activity occurs in the collagenase but not the blood infusion model of striatal hemorrhagic stroke in rats. Translational stroke research. 2015;6(1):29–38. doi:10.1007/s12975-014-0361-y. [PubMed: 25053257]
37. Wu G, Xi G, Hua Y, Sagher O. T2* magnetic resonance imaging sequences reflect brain tissue iron deposition following intracerebral hemorrhage. Translational stroke research. 2010;1(1):31–4. doi:10.1007/s12975-009-0008-6. [PubMed: 20811505]
38. Wan S, Cheng Y, Jin H, Guo D, Hua Y, Keep RF et al. Microglia Activation and Polarization After Intracerebral Hemorrhage in Mice: the Role of Protease-Activated Receptor-1. Translational stroke research. 2016;7(6):478–87. doi:10.1007/s12975-016-0472-8. [PubMed: 27206851]
39. Iniaghe LO, Krafft PR, Klebe DW, Omogbai EKI, Zhang JH, Tang J. Dimethyl fumarate confers neuroprotection by casein kinase 2 phosphorylation of Nrf2 in murine intracerebral hemorrhage. Neurobiology of disease. 2015;82:349–58. doi:10.1016/j.nbd.2015.07.001. [PubMed: 26176793]
40. Wang J, Tsirka SE. Tuftsin fragment 1–3 is beneficial when delivered after the induction of intracerebral hemorrhage. Stroke. 2005;36(3):613–8. doi:10.1161/01.STR.0000155729.12931.8f. [PubMed: 15692122]
41. Guo F, Hua Y, Wang J, Keep RF, Xi G. Inhibition of carbonic anhydrase reduces brain injury after intracerebral hemorrhage. Translational stroke research. 2012;3(1):130–7. doi:10.1007/s12975-011-0106-0. [PubMed: 22400066]
42. Miner JH, Patton BL, Lentz SI, Gilbert DJ, Snider WD, Jenkins NA et al. The laminin alpha chains: expression, developmental transitions, and chromosomal locations of alpha1–5, identification of heterotrimeric laminins 8–11, and cloning of a novel alpha3 isoform. J Cell Biol. 1997;137(3):685–701. [PubMed: 9151674]
43. Zudaire E, Gambardella L, Kurcz C, Vermeren S. A computational tool for quantitative analysis of vascular networks. PLoS One. 2011;6(11):e27385. doi:10.1371/journal.pone.0027385. [PubMed: 22110636]
44. Siqueira M, Francis D, Gisbert D, Gomes FCA, Stipursky J. Radial Glia Cells Control Angiogenesis in the Developing Cerebral Cortex Through TGF-beta1 Signaling. Mol Neurobiol. 2018;55(5):3660–75. doi:10.1007/s12035-017-0557-8. [PubMed: 28523566]

45. Salehi A, Jullienne A, Baghchechi M, Hamer M, Walsworth M, Donovan V et al. Up-regulation of Wnt/beta-catenin expression is accompanied with vascular repair after traumatic brain injury. J Cereb Blood Flow Metab. 2018;38(2):274–89. doi:10.1177/0271678X17744124. [PubMed: 29160735]
46. Manaenko A, Chen H, Kammer J, Zhang JH, Tang J. Comparison Evans Blue injection routes: Intravenous versus intraperitoneal, for measurement of blood-brain barrier in a mice hemorrhage model. J Neurosci Methods. 2011;195(2):206–10. doi:10.1016/j.jneumeth.2010.12.013. [PubMed: 21168441]
47. Lu X, Chen-Roetling J, Regan RF. Systemic hemin therapy attenuates blood-brain barrier disruption after intracerebral hemorrhage. Neurobiol Dis. 2014;70:245–51. doi:10.1016/j.nbd.2014.06.005. [PubMed: 24952361]
48. Ma Q, Huang B, Khatibi N, Rolland W 2nd, Suzuki H, Zhang JH et al. PDGFR-alpha inhibition preserves blood-brain barrier after intracerebral hemorrhage. Annals of neurology. 2011;70(6):920–31. doi:10.1002/ana.22549. [PubMed: 22190365]
49. Keep RF, Hua Y, Xi G. Brain water content. A misunderstood measurement? Translational stroke research. 2012;3(2):263–5. doi:10.1007/s12975-012-0152-2. [PubMed: 22888371]
50. Clark W, Gunion-Rinker L, Lessov N, Hazel K. Citicoline treatment for experimental intracerebral hemorrhage in mice. Stroke. 1998;29(10):2136–40. [PubMed: 9756595]
51. Wang J, Rogove AD, Tsirka AE, Tsirka SE. Protective role of tuftsin fragment 1–3 in an animal model of intracerebral hemorrhage. Ann Neurol. 2003;54(5):655–64. doi:10.1002/ana.10750. [PubMed: 14595655]
52. Kisanuki YY, Hammer RE, Miyazaki J, Williams SC, Richardson JA, Yanagisawa M. Tie2-Cre transgenic mice: a new model for endothelial cell-lineage analysis in vivo. Developmental biology. 2001;230(2):230–42. doi:10.1006/dbio.2000.0106. [PubMed: 11161575]
53. Constien R, Forde A, Liliensiek B, Grone HJ, Nawroth P, Hammerling G et al. Characterization of a novel EGFP reporter mouse to monitor Cre recombination as demonstrated by a Tie2 Cre mouse line. Genesis. 2001;30(1):36–44. [PubMed: 11353516]
54. Tang Y, Harrington A, Yang X, Friesel RE, Liaw L. The contribution of the Tie2+ lineage to primitive and definitive hematopoietic cells. Genesis. 2010;48(9):563–7. doi:10.1002/dvg.20654. [PubMed: 20645309]
55. Bazzoni G, Dejana E. Endothelial cell-to-cell junctions: molecular organization and role in vascular homeostasis. Physiol Rev. 2004;84(3):869–901. doi:10.1152/physrev.00035.2003 84/3/869 [pii]. [PubMed: 15269339]
56. Kniesel U, Wolburg H. Tight junctions of the blood-brain barrier. Cellular and molecular neurobiology. 2000;20(1):57–76. [PubMed: 10690502]
57. Daneman R, Zhou L, Kebede AA, Barres BA. Pericytes are required for blood-brain barrier integrity during embryogenesis. Nature. 2010;468(7323):562–6. doi:10.1038/nature09513 nature09513 [pii]. [PubMed: 20944625]
58. Armulik A, Genove G, Mae M, Nisancioglu MH, Wallgard E, Niaudet C et al. Pericytes regulate the blood-brain barrier. Nature. 2010;468(7323):557–61. doi:nature09522 [pii] 10.1038/nature09522. [PubMed: 20944627]
59. Bell RD, Winkler EA, Sagare AP, Singh I, LaRue B, Deane R et al. Pericytes control key neurovascular functions and neuronal phenotype in the adult brain and during brain aging. Neuron. 2010;68(3):409–27. doi:S0896-6273(10)00824-X [pii] 10.1016/j.neuron.2010.09.043. [PubMed: 21040844]
60. Bell RD, Winkler EA, Singh I, Sagare AP, Deane R, Wu Z et al. Apolipoprotein E controls cerebrovascular integrity via cyclophilin A. Nature. 2012;485(7399):512–6. doi:10.1038/nature11087 nature11087 [pii]. [PubMed: 22622580]
61. Bernacki J, Dobrowolska A, Nierwinska K, Malecki A. Physiology and pharmacological role of the blood-brain barrier. Pharmacol Rep. 2008;60(5):600–22. [PubMed: 19066407]
62. Bian GL, Wei LC, Shi M, Wang YQ, Cao R, Chen LW. Fluoro-Jade C can specifically stain the degenerative neurons in the substantia nigra of the 1-methyl-4-phenyl-1,2,3,6-tetrahydro pyridine-treated C57BL/6 mice. Brain research. 2007;1150:55–61. doi:10.1016/j.brainres.2007.02.078. [PubMed: 17397812]

63. Sukumari-Ramesh S, Alleyne CH Jr., Dhandapani KM. Astrocyte-specific expression of survivin after intracerebral hemorrhage in mice: a possible role in reactive gliosis? Journal of neurotrauma. 2012;29(18):2798–804. doi:10.1089/neu.2011.2243. [PubMed: 22862734]
64. Wasserman JK, Yang H, Schlichter LC. Glial responses, neuron death and lesion resolution after intracerebral hemorrhage in young vs. aged rats. The European journal of neuroscience. 2008;28(7):1316–28. doi:10.1111/j.1460-9568.2008.06442.x. [PubMed: 18973558]
65. Ohsawa K, Imai Y, Kanazawa H, Sasaki Y, Kohsaka S. Involvement of Iba1 in membrane ruffling and phagocytosis of macrophages/microglia. J Cell Sci. 2000;113 (Pt 17):3073–84. [PubMed: 10934045]
66. Jeong HK, Ji K, Min K, Joe EH. Brain inflammation and microglia: facts and misconceptions. Exp Neurobiol. 2013;22(2):59–67. doi:10.5607/en.2013.22.2.59. [PubMed: 23833554]
67. Song J, Zhang X, Buscher K, Wang Y, Wang H, Di Russo J et al. Endothelial basement membrane laminin 511 contributes to endothelial junctional tightness and thereby inhibits leukocyte transmigration. Cell reports. 2017;18(5):1256–69. [PubMed: 28147279]
68. Song J, Lokmic Z, Lämmermann T, Rolf J, Wu C, Zhang X et al. Extracellular matrix of secondary lymphoid organs impacts on B-cell fate and survival. Proceedings of the National Academy of Sciences. 2013;110(31):E2915–E24.
69. Wang S, Voisin MB, Larbi KY, Dangerfield J, Scheiermann C, Tran M et al. Venular basement membranes contain specific matrix protein low expression regions that act as exit points for emigrating neutrophils. The Journal of experimental medicine. 2006;203(6):1519–32. doi:10.1084/jem.20051210. [PubMed: 16754715]
70. Voisin MB, Probstl D, Nourshargh S. Venular basement membranes ubiquitously express matrix protein low-expression regions: characterization in multiple tissues and remodeling during inflammation. The American journal of pathology. 2010;176(1):482–95. doi:10.2353/ajpath.2010.090510. [PubMed: 20008148]
71. Warren KJ, Iwami D, Harris DG, Bromberg JS, Burrell BE. Laminins affect T cell trafficking and allograft fate. The Journal of clinical investigation. 2014;124(5):2204–18. doi:10.1172/JCI73683. [PubMed: 24691446]
72. Yanaka K, Camarata PJ, Spellman SR, Skubitz AP, Furcht LT, Low WC. Laminin peptide ameliorates brain injury by inhibiting leukocyte accumulation in a rat model of transient focal cerebral ischemia. J Cereb Blood Flow Metab. 1997;17(6):605–11. doi:10.1097/00004647-199706000-00002. [PubMed: 9236717]
73. Chen ZL, Strickland S. Neuronal death in the hippocampus is promoted by plasmin-catalyzed degradation of laminin. Cell. 1997;91(7):917–25. [PubMed: 9428515]
74. Chen ZL, Indyk JA, Strickland S. The hippocampal laminin matrix is dynamic and critical for neuronal survival. Mol Biol Cell. 2003;14(7):2665–76. doi:10.1091/mbc.e02-12-0832. [PubMed: 12857855]
75. Omar MH, Kerrisk Campbell M, Xiao X, Zhong Q, Brunken WJ, Miner JH et al. CNS Neurons Deposit Laminin alpha5 to Stabilize Synapses. Cell Rep. 2017;21(5):1281–92. doi:10.1016/j.celrep.2017.10.028. [PubMed: 29091766]
76. Johnson KM, Milner R, Crocker SJ. Extracellular matrix composition determines astrocyte responses to mechanical and inflammatory stimuli. Neuroscience letters. 2015;600:104–9. doi:10.1016/j.neulet.2015.06.013. [PubMed: 26067407]
77. Biswas S, Bachay G, Chu J, Hunter DD, Brunken WJ. Laminin-Dependent Interaction between Astrocytes and Microglia: A Role in Retinal Angiogenesis. The American journal of pathology. 2017;187(9):2112–27. doi:10.1016/j.ajpath.2017.05.016. [PubMed: 28697326]
78. Tam WY, Au NPB, Ma CHE. The association between laminin and microglial morphology in vitro. Scientific reports. 2016;6:28580. [PubMed: 27334934]
79. Yao Y, Tsirka SE. Chemokines and their receptors in intracerebral hemorrhage. Translational stroke research. 2012;3(Suppl 1):70–9. doi:10.1007/s12975-012-0155-z. [PubMed: 24323863]
80. Ropper AH, Zervas NT. Cerebral blood flow after experimental basal ganglia hemorrhage. Ann Neurol. 1982;11(3):266–71. doi:10.1002/ana.410110306. [PubMed: 7092179]

81. Deinsberger W, Vogel J, Kuschinsky W, Auer LM, Boker DK. Experimental intracerebral hemorrhage: description of a double injection model in rats. Neurol Res. 1996;18(5):475–7. [PubMed: 8916066]
82. Rosenberg GA, Mun-Bryce S, Wesley M, Kornfeld M. Collagenase-induced intracerebral hemorrhage in rats. Stroke. 1990;21(5):801–7. [PubMed: 2160142]
83. Krafft PR, Rolland WB, Duris K, Lekic T, Campbell A, Tang J et al. Modeling intracerebral hemorrhage in mice: injection of autologous blood or bacterial collagenase. J Vis Exp. 2012(67):e4289. doi:10.3791/4289. [PubMed: 23023153]
84. Tang J, Liu J, Zhou C, Alexander JS, Nanda A, Granger DN et al. Mmp-9 deficiency enhances collagenase-induced intracerebral hemorrhage and brain injury in mutant mice. Journal of cerebral blood flow and metabolism : official journal of the International Society of Cerebral Blood Flow and Metabolism. 2004;24(10):1133–45. doi:10.1097/01.WCB.0000135593.05952.DE.
85. Manaenko A, Chen H, Zhang JH, Tang J. Comparison of different preclinical models of intracerebral hemorrhage. Acta Neurochir Suppl. 2011;111:9–14. doi: 10.1007/978-3-7091-0693-8_2. [PubMed: 21725724]
86. MacLellan CL, Davies LM, Fingas MS, Colbourne F. The influence of hypothermia on outcome after intracerebral hemorrhage in rats. Stroke; a journal of cerebral circulation. 2006;37(5):1266–70. doi:10.1161/01.STR.0000217268.81963.78.
87. Brown MS, Kornfeld M, Mun-Bryce S, Sibbitt RR, Rosenberg GA. Comparison of magnetic resonance imaging and histology in collagenase-induced hemorrhage in the rat. J Neuroimaging. 1995;5(1):23–33. [PubMed: 7849368]
88. Gazendam J, Houthoff HJ, Huitema S, Go KG. Cerebral Edema Formation and Blood-Brain Barrier Impairment by Intraventricular Collagenase Infusion In: Go KG, Baethmann A, editors. Recent Progress in the Study and Therapy of Brain Edema. Boston, MA: Springer US; 1984 p. 159–73.
89. Rosenberg GA, Estrada E, Kelley RO, Kornfeld M. Bacterial collagenase disrupts extracellular matrix and opens blood-brain barrier in rat. Neurosci Lett. 1993;160(1):117–9. [PubMed: 8247322]
90. James ML, Warner DS, Laskowitz DT. Preclinical Models of Intracerebral Hemorrhage: A Translational Perspective. Neurocritical Care. 2007;9(1):139. doi:10.1007/s12028-007-9030-2.
91. MacLellan CL, Silasi G, Auriat AM, Colbourne F. Rodent models of intracerebral hemorrhage. Stroke. 2010;41(10 Suppl):S95–8. doi:10.1161/STROKEAHA.110.594457. [PubMed: 20876518]
92. Xue M, Del Bigio MR. Intracerebral injection of autologous whole blood in rats: time course of inflammation and cell death. Neurosci Lett. 2000;283(3):230–2. [PubMed: 10754230]
93. MacLellan CL, Auriat AM, McGie SC, Yan RH, Huynh HD, De Butte MF et al. Gauging recovery after hemorrhagic stroke in rats: implications for cytoprotection studies. J Cereb Blood Flow Metab. 2006;26(8):1031–42. doi:10.1038/sj.jcbfm.9600255. [PubMed: 16395282]
94. Gong C, Hoff JT, Keep RF. Acute inflammatory reaction following experimental intracerebral hemorrhage in rat. Brain Res. 2000;871(1):57–65. [PubMed: 10882783]

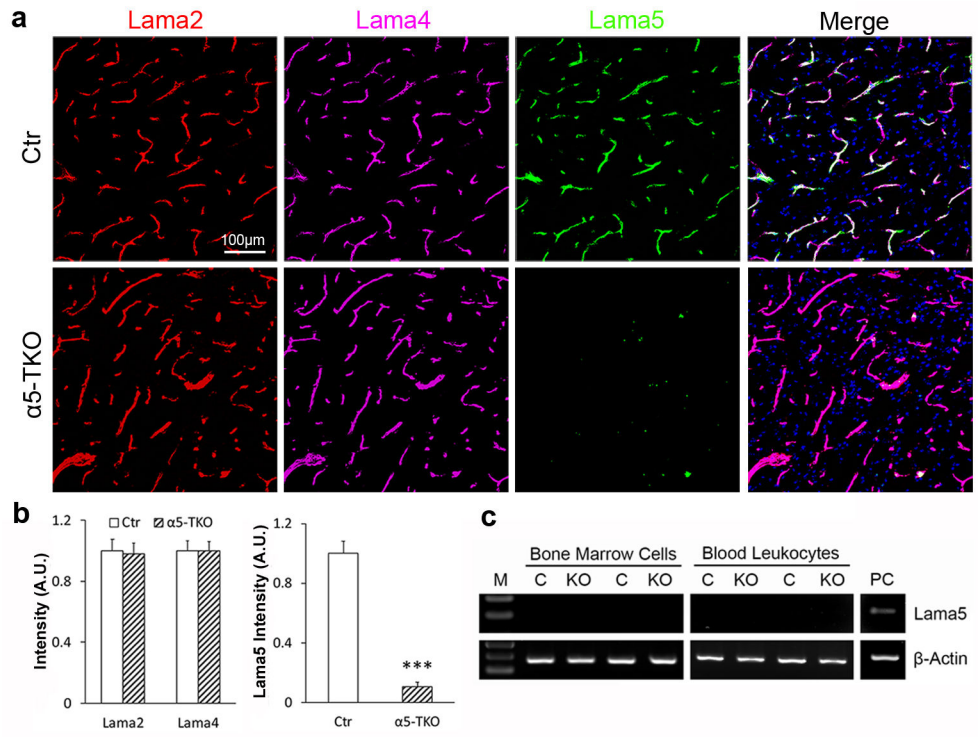

Fig. 1.

Lama5 is selectively ablated in endothelial cells in α5-TKO mice. **a** Representative images of laminin α2 (red), laminin α4 (magenta) and laminin α5 (green) staining in control and α5-TKO brains. **b** Quantifications of laminin α2, laminin α4, and laminin α5 intensity in these mice. n=4. Student's t-test was used for statistical analyses. **c** RT-PCR analysis of lama5 and β-Actin expression in bone marrow cells and peripheral blood leukocytes from control and α5-TKO mice. M, marker; C, control; KO, α5-TKO; PC, positive control. ***$p < 0.001$, compared to wildtype controls.

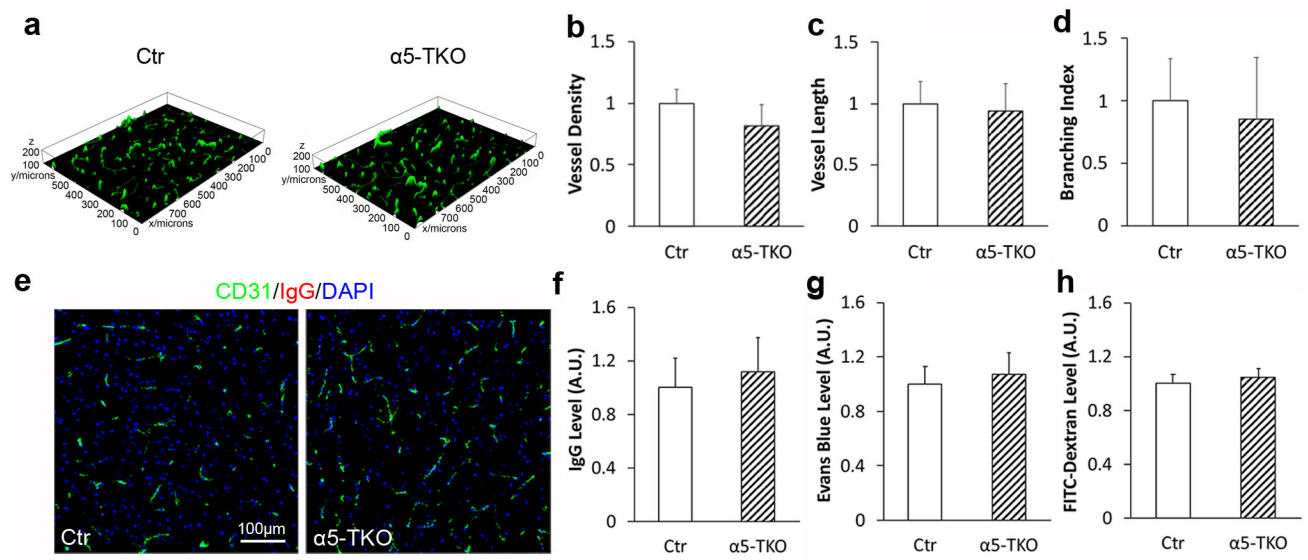

Fig. 2.

Brain angioarchitecture and BBB integrity are unaffected in α5-TKO mice under homeostatic conditions. **a** Representative 3D images of IB4 (green) staining in control and α5-TKO brains. **b-d** Quantifications of vessel density (**b**), vessel length (**c**), and branching index (**d**) in control and α5-TKO brains. n=3. Student's t-test was used for statistical analyses. **e** Representative images of CD31 (green) and IgG (red) staining in control and α5-TKO brains. **f-h** Quantifications of IgG (**f**), Evans blue (**g**), and FITC-Dextran (**h**) levels in the brains of these mice. n=4. Student's t-test was used for statistical analyses.

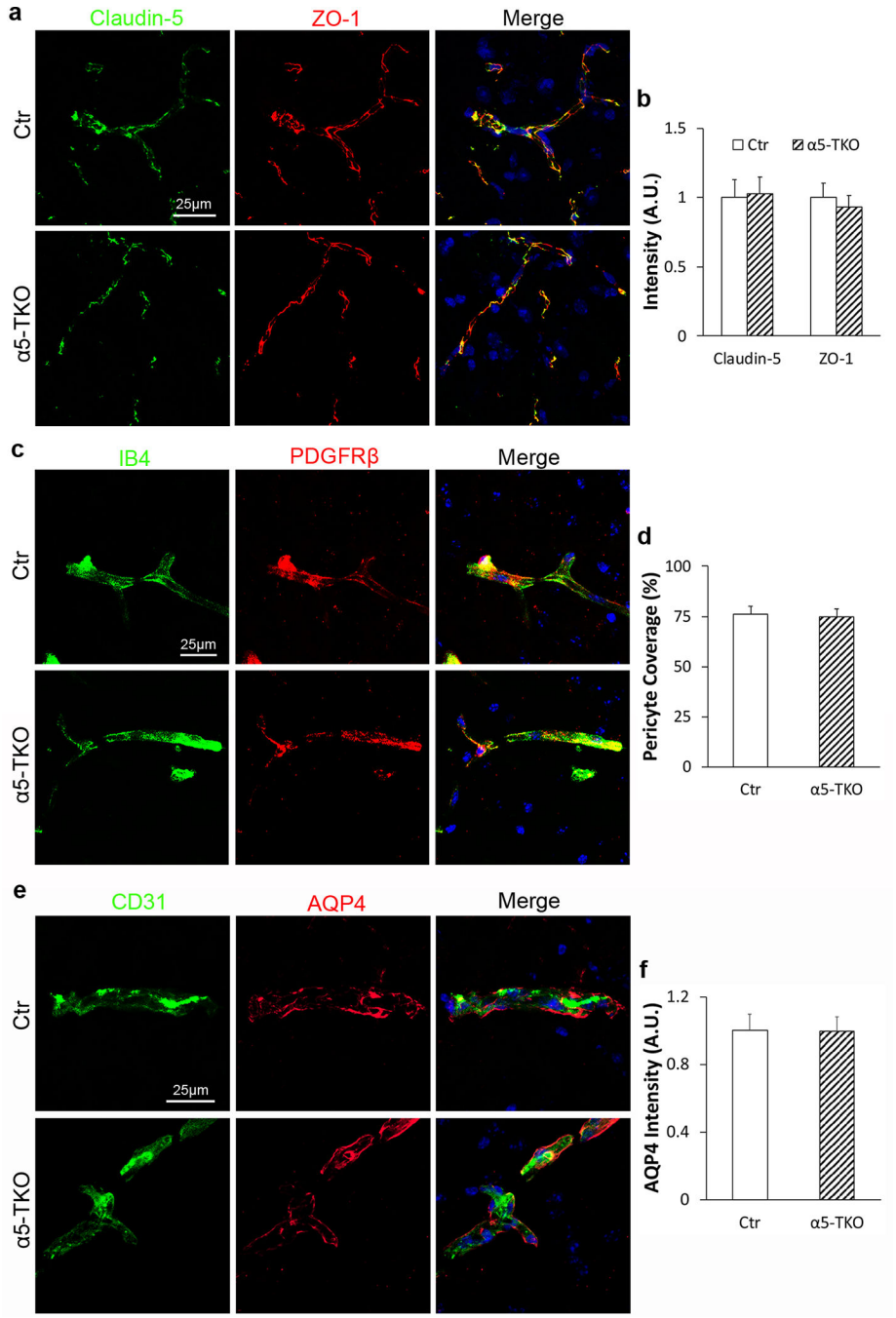

Fig. 3.

α5-TKO mice show no defects in TJP expression, pericyte coverage, and astrocyte polarity. **a** Representative images of Claudin-5 (green) and ZO-1 (red) staining in control and α5-TKO brains. **b** Quantifications of Claudin-5 and ZO-1 intensity in the brains of these mice. n=4. Student's t-test was used for statistical analyses. **c** Representative images of IB-4 (green) and PDGFRβ (red) staining in control and α5-TKO brains. **d** Quantification of pericyte coverage in the brains of these mice. n=4. Student's t-test was used for statistical analyses. **e** Representative images of CD31 (green) and AQP4 (red) staining in control and

α5-TKO brains. **f** Quantification of AQP4 intensity in the brains of control and α5-TKO mice. n=4. Student's t-test was used for statistical analyses.

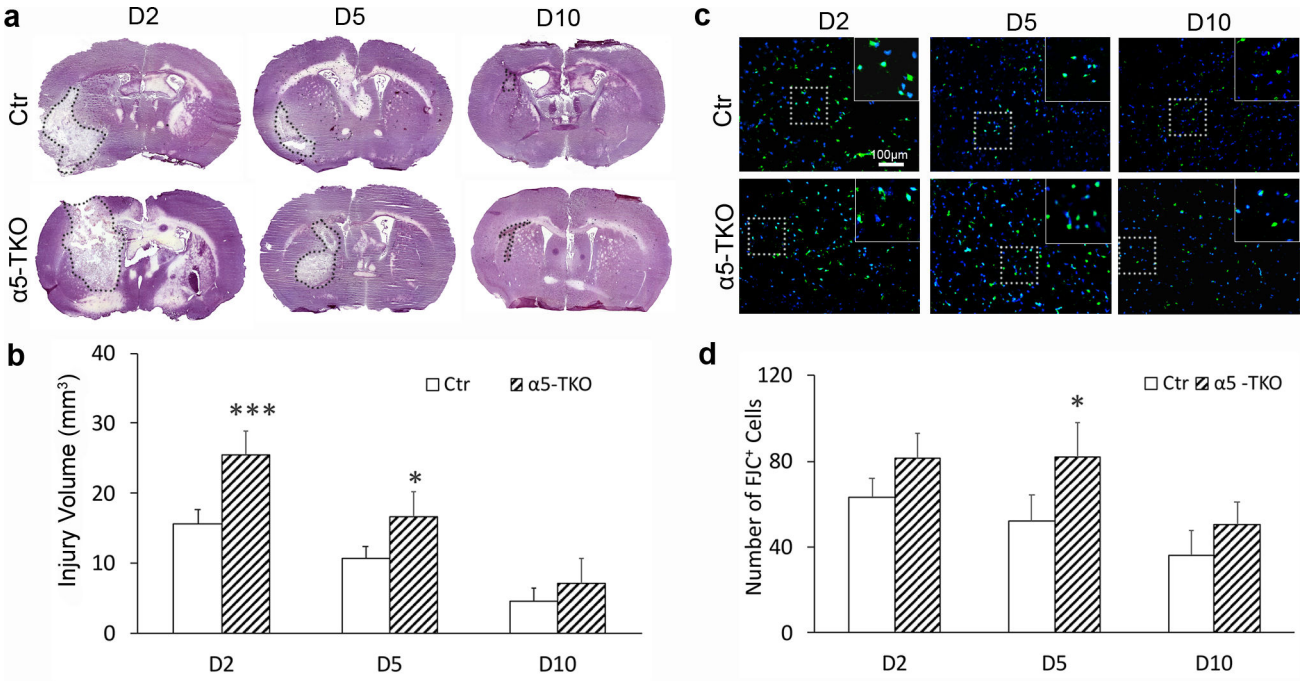

Fig. 4.

α5-TKO mice demonstrate enhanced injury volume and increased neuronal death after ICH. **a** Representative images of hematoxylin staining in control and α5-TKO brains at 2, 5, and 10 dpi. Dotted lines mark injury areas. **b** Quantifications of injury volume in these mice at 2, 5, and 10 dpi. n=4–5. One-Way ANOVA followed by Newman-Keuls test was used for statistical analyses. **c** Representative images of FJC staining in control and α5-TKO mice at 2, 5, and 10 dpi. **d** Quantifications of FJC^+ cells in these mice at 2, 5, and 10 dpi. n=3–4. One-Way ANOVA followed by Newman-Keuls test was used for statistical analyses. $*p < 0.05$, $***p < 0.001$; compared to controls at the same time points.

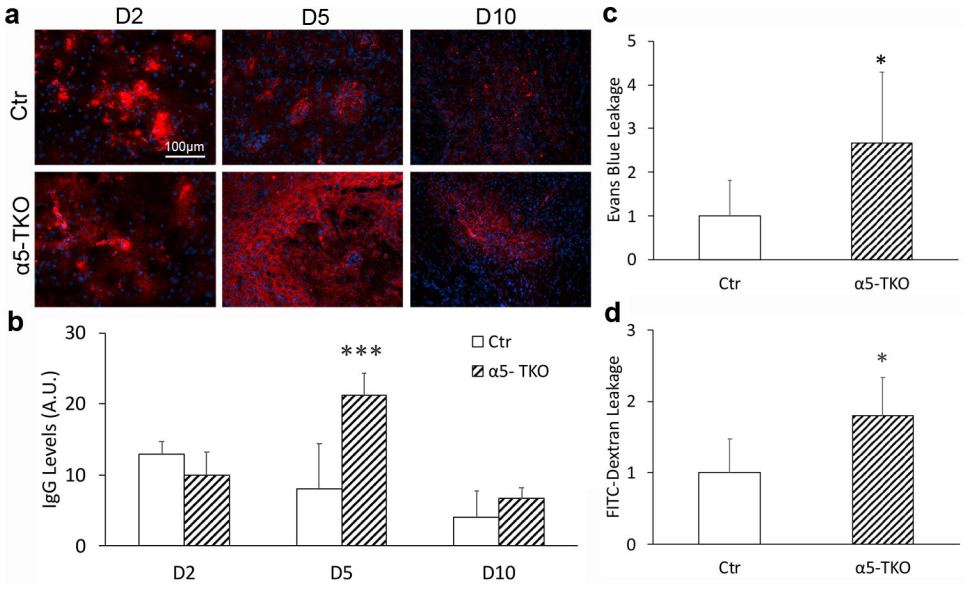

Fig. 5.

α5-TKO mice have exacerbated BBB disruption after ICH. **a** Representative images of IgG (red) staining in control and α5-TKO brains at 2, 5, and 10 dpi. **b** Quantifications of IgG levels in these mice at 2, 5, and 10 dpi. n=3–5. One-Way ANOVA followed by Newman-Keuls test was used for statistical analyses. **c-d** Quantifications of Evans blue (**c**) and FITC-Dextran (**d**) leakage in control and α5-TKO mice at 5 dpi. n=5–9. Student's t-test was used for statistical analyses. *$p < 0.05$, ***$p < 0.001$; compared to controls at the same time points.

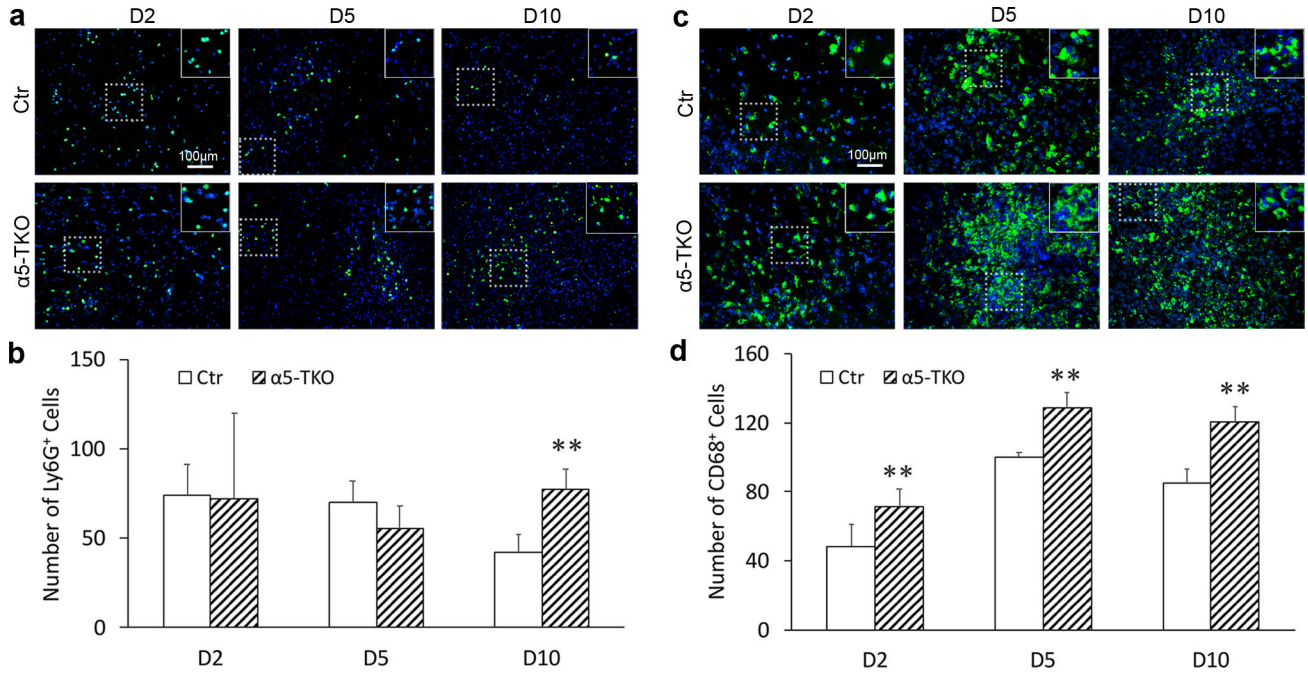

Fig. 6.

α5-TKO mice demonstrate increased inflammatory cell infiltration after ICH. **a** Immunohistochemistry of Ly6G in control and α5-TKO brains at 2, 5, and 10 dpi. **b** Quantification of $Ly6G^+$ neutrophils in control and α5-TKO mice at 2, 5, and 10 dpi. n=3–4. One-Way ANOVA followed by Newman-Keuls test was used for statistical analyses. **c** Immunohistochemistry of CD68 in control and α5-TKO brains at 2, 5, and 10 dpi. **d** Quantification of $CD68^+$ monocytes/macrophages in control and α5-TKO mice at 2, 5, and 10 dpi. n=3–4. One-Way ANOVA followed by Newman-Keuls test was used for statistical analyses. $^{**}p < 0.01$, compared to controls at the same time points.

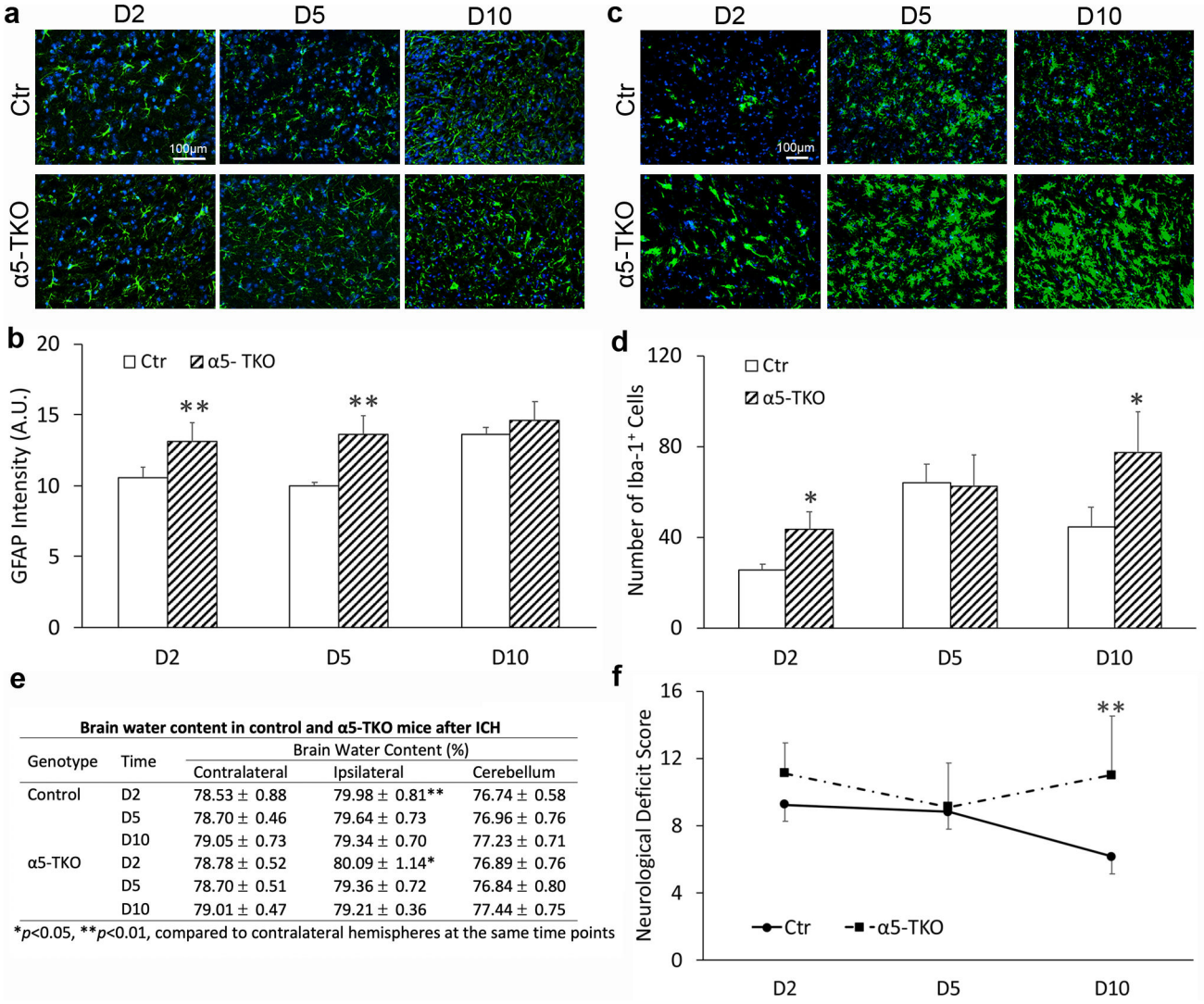

Brain water content in control and α5-TKO mice after ICH

Genotype	Time	Brain Water Content (%)		
		Contralateral	Ipsilateral	Cerebellum
Control	D2	78.53 ± 0.88	79.98 ± 0.81**	76.74 ± 0.58
	D5	78.70 ± 0.46	79.64 ± 0.73	76.96 ± 0.76
	D10	79.05 ± 0.73	79.34 ± 0.70	77.23 ± 0.71
α5-TKO	D2	78.78 ± 0.52	80.09 ± 1.14*	76.89 ± 0.76
	D5	78.70 ± 0.51	79.36 ± 0.72	76.84 ± 0.80
	D10	79.01 ± 0.47	79.21 ± 0.36	77.44 ± 0.75

*p<0.05, **p<0.01, compared to contralateral hemispheres at the same time points

Fig. 7.

α5-TKO mice have increased astrocyte/microglial activation, unchanged brain water content, and worse neurological function after ICH. **a** Immunohistochemistry of GFAP in control and α5-TKO brains at 2, 5, and 10 dpi. **b** Quantification of GFAP intensity in control and α5-TKO mice at 2, 5, and 10 dpi. n=3. One-Way ANOVA followed by Newman-Keuls test was used for statistical analyses. **c** Immunohistochemistry of Iba-1 in control and α5-TKO brains at 2, 5, and 10 dpi. **d** Quantification of Iba-1$^+$ microglia number in control and α5-TKO mice at 2, 5, and 10 dpi. n=3. One-Way ANOVA followed by Newman-Keuls test was used for statistical analyses. **e** Quantification of brain water content in control and α5-TKO mice at 2, 5, and 10 dpi. n=6–9. One-Way ANOVA followed by Newman-Keuls test was used for statistical analyses. **f** Neurological deficit score in control and α5-TKO mice at 2, 5, and 10 dpi. n=7–17. One-Way ANOVA followed by Newman-Keuls test was used for statistical analyses. *$p < 0.05$, **$p < 0.01$, compared to controls at the same time points in **b**, **d**, **f**; and compared to contralateral hemispheres at the same time points in **e**.